UNIVERSITY of
BRADFORD

Library

The University of Bradford Institutional Repository

http://bradscholars.brad.ac.uk

Link to publisher's version: *http://dx.doi.org/10.1016/j.jfoodeng.2016.08.005*

Citation: Al-Obaidi MA, Kara-Zaitri KM and Mujtaba IM (2017) Development of a mathematical model for apple juice compounds rejection in a spiral-wound reverse osmosis process. Journal of Food Engineering. 192: 111-121.

Development of a Mathematical Model for Apple Juice Compounds Rejection in a Spiral-wound Reverse Osmosis Process

Al-Obaidi M. A., Kara-Zaïtri C. and Mujtaba I. M. *

School of Engineering, Faculty of Engineering and Informatics. University of Bradford, Bradford, West Yorkshire BD7 1DP, UK

*Corresponding author, Tel.: +44 0 1274 233645

E-mail address: I.M.Mujtaba@bradford.ac.uk

Abstract

The use of Reverse Osmosis (RO) membrane processes for the clarification and the concentration of apple juice is proposed as an alternative to the conventional concentration technique, which is based on evaporation and freezing. Several models have been published on RO process models relying on different assumptions that predict the permeate flux and aroma compounds rejections for aqueous solutions apple juice. The solution-diffusion model (Lumped model) has been applied for the previous models. The main instrument of this study is the use of the gPROMS software to develop a new distributed steady state model that will relax a number of earlier assumptions.

The model has been validated with an observational data of apple juice filtration derived from the literature by analysing the permeate flux and the performance of membrane rejection at different concentrations, temperatures and pressures for a laboratory scale of spiral-wound RO module. Simulated results corroborate with experimental and model predictions.

*Keywords***:** Apple Juice Concentration; Spiral-wound Reverse Osmosis; One Dimensional Distributed Model; gPROMS software.

1. Introduction

The concentration of fruit juices is achieved by reducing the water content. This has many advantages, including easier and cheaper conservation, storage, transportation and distribution of the extracted juice. Conventional methods of fruit juices concentration are usually conducted using a high temperature multi-stage vacuum evaporation process. This process usually results in significant losses of nutritional compounds, such as vitamin C, as well as associated thermal effects (Pozderovic´ et al. 2006). As a result, RO has become an alternative process to the conventional methods for removing water from fruit juices and other liquid foods (Girard and Fukumoto, 2000). However, one of the main disadvantages of using RO is related to lower concentration of the yield in comparison to the thermal process due to high osmotic pressure limitation. Having said this, the RO process has affirmed its

35 potential as the prominent process for retaining the aroma compounds (Jiao et al., 2004).

36 Therefore, the RO process is a well-recognized technique for concentrating aqueous solutions

37 within a limit of 25 to 30 °Brix, which is quite below the typical value of 45 to 60 °Brix gain

38 by the evaporation process (Pepper, 1990). With the aim to improve the concentration and yet

39 retain the critical aroma feature, this research proposes a RO process but one that is used as a

40 pre-concentration step with other technologies (Sheu and Wiley, 1983).

41 Due to the obvious high commercial implications, several attempts can be found in the

42 literature to improve the concentration of apple juice. Many such models are based on the RO

43 process in order to measure permeate flux and to elucidate the rejection of one component

44 and multi-component fruit solutions. A critique on the current literature is discussed in the

45 following section.

46 Nabetani et al. (1992a) have proposed a new correlation to estimate the osmotic pressure of

47 sucrose and glucose solution using thermodynamic definition of the osmotic pressure. The

48 proposed equations assume that the osmotic pressure can be expressed in terms of solute

49 concentration. Accordingly, Nabetani et al. (1992b) have developed a model using the

50 combination of sucrose and glucose osmotic pressure developed in Nabetani et al. (1992a)

51 with the solution-diffusion model equations. The model can predict the permeation of apple

52 juice solution considering the solution physical properties of both one component and a

53 binary solute solution. The model has been validated for a tubular RO module type (ZF 99)

54 supplied by PCI (Paterson Candy International, England) and shows a good agreement

55 between experimental RO data and those calculated on the basis of the solution-diffusion

56 model. However, this particular model considered only sucrose and glucose solute

57 concentration in the bulk retentate with ignored the permeate concentration.

58 Álvarez et al. (1997) have used the solution-diffusion model and the film theory with the

59 proposed osmotic pressure of Nabetani et al. (1992b) to predict the permeate flux in apple

60 juice concentration. This was done by using a tubular polyamide RO membrane type (AFC

61 99) supplied by PCI (Paterson Candy International, England). The model incorporates the

62 physico-chemical correlations to evaluate the characteristics of concentrated apple juice.

63 However, the model ignored the solute concentration at the permeate side and degraded the

64 osmotic pressure caused by fructose and sorbitol in spite of taking into account the

65 contribution of sucrose, glucose and malic acid to the osmotic pressure. Furthermore, Álvarez

66 et al. (1998) used the procedure developed by Matsuura et al. (1974) to calculate the solute

67 transport parameter for each aroma compound for a spiral-wound RO aromatic polyamide

68 membrane type (MSCB 2521 R99) supplied by Separem Spa. (Biella, Italy). Table 1 reports

69 the values of free energy parameter, steric Taft number and solute transport parameter for

70 each aroma compound. Then, the solution-diffusion model is used to estimate the rejection of

71 hydrophilic aroma compounds by considering the average value of inlet feed and retentate as

72 the concentration of bulk solution, but overlooked the osmotic pressure. After that, Álvarez et

73 al. (2001) studied the rejection of aroma compounds using experimental data of solute

74 transport parameter for each aroma compounds calculated for the same above module of RO

75 membrane in the solution-diffusion model. Similarly, this work shows the influence of

76 temperature and feed flow rate on pure water permeability coefficient. The model studied was

77 used to predict the impact of operating conditions such as feed flow rate and concentration on

78 the permeate flux and aroma compound rejections. However, feed osmotic pressure is

79 referred only to glucose.

80 Álvarez et al. (2002) have used the same procedure developed in the work shown above to

81 predict the aroma compounds rejection and the permeate flux during the reverse osmosis

82 concentration of apple juice at laboratory and pilot-scales of MSCB 2521 R99 and MSCE

83 4040 R99 spiral wound membrane supplied by Separem Spa. (Biella, Italy) respectively. The

84 model can predict the influence of operating conditions on permeate flux and aroma

85 compounds rejection. However, this work not only ignored the contribution of fructose and

86 sorbitol in feed osmotic pressure, but also neglected the concentration at the permeate side.

87 To the best of authors' knowledge, all the published RO process modelling for the

88 concentration of apple juice has been carried out using the entire arrangement as a black box

89 and simply taking average inputs and outputs parameter values. In this paper, the finite

90 difference approach is used instead as it gives more accurate results because it takes into

91 account the variation of the operating parameters along the entire system. Also, the above

92 studies have been proposed to describe flux behaviour and compounds retention by relying

93 on the assumption that the osmotic pressure of sugar is only caused by glucose, sucrose and

94 malic acid, and thus ignoring fructose and sorbitol. Pereira et al. (1976) confirmed that

95 glucose and fructose have greater mass transfer and solute transport characteristics than that

96 of sucrose. To systematically resolve this problem, the scope of this paper is to present the

97 development of a distributed one dimensional steady state model and define and asses the

98 variation of the operating conditions as a function of position along the x-axis of the spiral-

99 wound module in the process of apple juice filtration. As well as this, the contribution of all

100   sugar species in the feed osmotic pressure will be taken into consideration. The validation of

101   this model will be based on a comparison between simulation and experimental results

102   derived from the literature. The process model developed can be used later to assess the

103   operating conditions and system design in order to optimize the concentration of apple juice

104   and the retention of aroma compounds.

105   **2. The Main Principles**

106   Reverse Osmosis can be defined as a process of removing undesirable species (salts,

107   pollutants, etc.) from liquid solutions (seawater, wastewater, etc.) by pumping the solution at

108   a hydraulic pressure greater than the osmotic pressure within a closed vessel to move water

109   from high solute side to the diluted side (Jain et al., 2004). There does not appear to be a

110   widespread agreement on the mechanisms of water and solute transport through RO

111   membrane for aqueous solutes (Girard and Fukumoto, 2000). However, the most accepted

112   approaches in this respect are the Solution-diffusion and Preferential sorption theories. The

113   first theory assumes that solvent and solute dissolve in the membrane and pass through by

114   diffusion, while the second theory assumes that solvent and solute are adsorbed at the

115   membrane surface and then pass through the membrane pores.

116   Generally, as the water is removed and the solute is rejected and accumulated at the

117   membrane surface, the water flux drops due to an increase in the osmotic pressure of the feed

118   and concentration polarization impact. There are considered as the main factors causing flux

119   deterioration. These impediments can be fixed by altering the operating condition such as,

120   feed pressure, concentration, temperature and cross-flow velocity and also by turbulence

121   promotion, back flushing/washing and pulsed flow.

122   Normally, a solution treated by RO in food industries is considered as a multi-component

123   solution, which contains a number of solutes at different concentrations. Specifically, apple

124   juice comprises two groups of organic compounds; sugar and aroma compounds, which are

125   categorized as esters (the main compound), aldehydes and alcohols. Also, aroma is one of the

126   most appreciated fresh fruit juice flavor characteristics and is of great importance by

127   consumers. Aroma is due to a large number of volatile organic compounds present in

128   different concentrations, which play a key role in customer perception and satisfaction

129   (Cheong et al., 2010).

130
131
132
133
134

2. Materials and Methods

2.1 Apple Juice Characteristics

Table 1 shows the composition and concentration of the apple juice (sugar and aroma compounds) used by Álvarez et al. (2002) in all of the experiments as the feed with concentration 10.5 ± 0.5 °Brix. The solution was prepared from 72 °Brix concentrated apple juice supplied by the apple processing company Valle, Ballina and Férnandez, S. A. (Villaviciosa, Spain), by adding distilled water.

2.2 Membrane Module Characteristics and Operating Conditions

The RO system used in all of the experiments conducted by Álvarez et al. (2002) was designed in a laboratory scale experiment consisting of a MSCB 2521 R99 spiral-wound aromatic polyamide membrane module supplied by Sparem Spa. (Biella, Italy). The detail of the manufacturer's specification membrane module is presented in Table 2. Experiments are carried out using a batch operation mode where the standard flow configuration of the feed volume is plug flow (passes once time through the system) and the concentrate retentate is recycled back to the feed tank to achieve high system recovery. In addition, permeate was recycled back to the feed tank to maintain a constant concentration and then removed from the equipment which concentration was increased. Experiments are implemented at three different trans-membrane pressures of 14.8, 24.673 and 34.542 atm within 20 to 30 °C , while the used inlet feed flow rate are 5.5556E-5, 1.111E-4 and 1.6667E-4 m³/s respectively.

3. Model Rationale and Development

3.1 Assumptions

A number of reasonable assumptions and simplifications are used in order to develop this model. They include:

1. The module is made up of porous flat sheet with spacers and negligible leaf curvature.

2. Validity of the solution-diffusion model for the transport of the solvent and solutes through the membrane.

162   3. Validity of the Darcy's law for the feed and permeate channels, which assumes that

163   the pressure drop is proportional to the feed and permeate flow rate and the friction

164   parameter is applied to characterize the pressure drop.

165   4. Validity of the film model theory to estimate the concentration polarization impact.

166   5. The feed osmotic pressure is caused by the impact of all the species found in sugar

167   and not restricted to only sucrose, glucose and malic acid.

168   6. Constant pressure of 1 atm on the permeate side.

169   7. Complete mixing in the y-axis of the feed channel due to the existence of a network of

170   spacers.

171   8. The underlying process is assumed to be isothermal.

172

173 **3.2 Model Structure**

174 A computational one dimensional model was developed in this study to predict the variation

175 of operating parameters and permeate flux in the x-axis during the reverse osmosis

176 concentration of apple juice at laboratory scale spiral-wound RO process.

177 The details of model development, the equations and the physic-chemical properties of apple

178 juice used throughout the simulation study are described below.

179 Based on Assumption 2, the solution-diffusion model is valid to predict the permeate flux

180 through the membrane at any point along the x-axis as expressed by the following equation

181 (Lonsdale et al., 1965).

182 $$J_{w(x)} = A_w \left(\Delta P_{b_{(x)}} - \Delta \pi_{Total,(x)} \right) \tag{1}$$

183 A_w, $J_{w(x)}$ (m/s, m/ s atm) are the water flux at any point along the x-axis and the membrane

184 permeability coefficient respectively. A_w was experimentally determined for the spiral-

185 wound module type (MSCB 2521 R99) using pure water and accounts for the pore

186 distribution of the membrane, porosity and membrane thickness. Álvarez et al. (2001)

187 introduce the following correlation to show the impact of feed flow rate and operating

188 temperature on A_w.

189 $$A_{w, T_b} = 9.059 x 10^{-7} \left(\frac{T_b}{25} \right)^{0.62} \left(\frac{36.0 x 10^5 \, F_{b(0)}}{400} \right)^{-0.1447} \tag{2}$$

190 The above equation confirms that the water permeability coefficient slightly decreased with

191 inlet feed flow rate and increased with temperature.

6

192 $(\Delta P_{b(x)} - \Delta \pi_{Total,(x)})$ is the quantity of force per unit area required to handle the osmotic

193 pressure and release pure water from the feed solution. $\Delta P_{b(x)}$ (atm) is the trans-membrane

194 pressure defined in Eq. (3).

195 $$\Delta P_{b(x)} = \left(P_{b(x)} - P_p \right) \tag{3}$$

196 $P_{b(x)}$, P_p are the feed pressure at any point along the x-axis and the constant permeate pressure

197 (Assumption 6) respectively. While, the overall trans-membrane pressure (TMP) (atm) for

198 each run is calculated as:

199 $$TMP = \frac{P_{b(0)} + P_{b(L)}}{2} - P_p \tag{4}$$

200 Where $P_{b(0)}$ and $P_{b(L)}$ (atm) are the pressure into the membrane and the pressure at the outlet

201 of the membrane respectively.

202 Because the aroma compounds concentration is very small compared to the sugar compounds

203 in apple juice (Table 1), $\Delta \pi_{Total,(x)}$ can only refer to the summation of the osmotic pressure

204 difference of sugar compounds along the length of the membrane. The osmotic pressure

205 difference of each sugar species can be defined as:

206 $$\Delta \pi_{(x)} = \pi_{Cw(x)} - \pi_{Cp(av)} \tag{5}$$

207 $\pi_{Cw(x)}$, $\pi_{Cp(av)}$ (atm) are the osmotic pressure of any sugar compound at the membrane wall

208 and permeate channel respectively.

209 Eq. (5) can be written as:

210 $$\Delta \pi_{(x)} = R\, T_b \left(C_{w(x)} - C_{p(av)} \right) \tag{6}$$

211 C_w and $C_{p(av)}$ (kmol/m³) are the solute concentration of sugar or aroma compounds at any

212 point along the x-axis at the membrane wall and average solute concentration at the permeate

213 side respectively. Also, R, T_b (atm L/K mol, K) are the gas constant and the apple juice

214 temperature respectively.

215 The solute flux $J_{s(x)}$ (kmol/m² s) of any sugar or aroma compounds along the x-axis can be

216 calculated as:

217 $$J_{s(x)} = B_s \left(C_{w(x)} - C_{p(av)} \right) \tag{7}$$

218 B_s (m/s) is the solute transport parameter of the determined species (sugar or aroma), which

219 is assumed as a constant along the length of the membrane and treated as unknown

220 parameters.

221 The solute flux is lower than volumetric solvent flux, and so $J_{s(x)}$ can be expressed as:

222 $$J_{s(x)} = J_{w(x)}\, C_{p(av)} \tag{8}$$

223   Eq. (6) can be written as:

224    $\Delta\pi_{(x)} = R\,T_b\,\dfrac{J_{s(x)}}{B_s}$ (9)

225   Substituting Eq. (8) in Eq. (9) and combining the result in Eq. (1) with re-arrangements yields

226   to Eq. (10).

227    $J_{w(x)} = \dfrac{A_w\,B_s\,\Delta P_{b(x)}}{B_s + A_w\,R\,T_b\,C_{p(av)}}$ (10)

228   Based on Assumption 6, Eq. (11) can readily be derived as:

229    $\dfrac{d\,\Delta P_{b(x)}}{dx} = \dfrac{d\,P_{b(x)}}{dx}$ (11)

230   Following on, Darcy's law can be used to express the feed pressure drop along the x-axis

231   according to Assumption 3.

232    $\dfrac{dP_{b(x)}}{dx} = -b\,F_{b(x)}$ (12)

233    $F_{b(x)}, b$ (m³/s, atm s/m⁴) are the feed flow rate at any point along the x-axis and the friction

234   parameter respectively. Taking the total mass balance based on the flow rate, gives:

235    $F_{b(0)} = F_{b(x)} + F_{p(x)}$ (13)

236    $F_{b(0)}, F_{p(x)}$ (m³/s) are the inlet feed flow rate and the permeate flow rate respectively. Also,

237   taking the total mass balance across a small section in the feed channel of the unit gives:

238    $\dfrac{dF_{b(x)}}{dx} = -\,W\,J_{w(x)}$ (14)

239   W (m) is the width of the membrane.

240   Furthermore, taking the derivative of Eq. (13) yields Eq. (15) to express the variation of

241   permeated flow rate along the x-axis as:

242    $\dfrac{dF_{b(x)}}{dx} = -\,\dfrac{dF_{p(x)}}{dx} = W\,J_{w(x)}$ (15)

243   Now, Dividing Eq. (12) and Eq. (14), yields:

244    $\dfrac{d\,\Delta P_{b(x)}}{dF_{b(x)}} = \dfrac{b\,F_{b(x)}}{W\,J_{w(x)}}$ (16)

245   The above equation can be written in the form of Eq. (17) by putting the value of solvent flux

246   from Eq. (10).

247    $F_{b(x)}\,dF_{b(x)} = \dfrac{W\,A_w\,B_s\,\Delta P_{b(x)}}{b\,\left(B_s + A_w\,R\,T_b\,C_{p(av)}\right)}\,d\Delta P_{b(x)}$ (17)

248   Further simplification, yields the following expression:

249    $F_{b(x)}\,dF_{b(x)} = \emptyset\;\Delta P_{b(x)}\,d\Delta P_{b(x)}$ (18)

250   Where, $\emptyset = \dfrac{W\,A_w\,B_s}{b\,\left(B_s + A_w\,R\,T_b\,C_{p(av)}\right)}$ (19)

251    $\emptyset$ is a parameter that can be calculated for all the sugar and aroma compounds and then the

252   average value will be considered as $\emptyset_{(mix)}$ for the rest of calculations.

253    $$\emptyset_{(mix)} = \frac{\sum_{i=1}^{n} \frac{W \, A_W \, B_S}{b \left(B_S + A_W \, R \, T_b \, C_{p(av)} \right)}}{n} \qquad (20)$$

254   where, n = Total number of sugar and aroma compounds

255   Re-arrangement with integration of Eq. (18) gives a correlation to calculate the feed flow rate

256   at any point along the x-axis as follows:

257    $$F_{b(x)} = F_{b(0)} + \emptyset^{0.5}_{(mix)} \left(\Delta P_{b(x)} - \Delta P_{b(0)} \right) \qquad (21)$$

258   Substituting Eq. (21) into Eq. (12) and taking the integration facilitates the calculation of the

259   trans-membrane pressure in any point along the x-axis.

260    $$\Delta P_{b(x)} = \Delta P_{b(0)} - b \, x \, F_{b(0)} - b \, x \, \Delta P_{b(x)} \left(\emptyset_{(mix)} \right)^{0.5} + b \, x \, \Delta P_{b(0)} \left(\emptyset_{(mix)} \right)^{0.5} \qquad (22)$$

261   Substituting Eqs. (20) and (22) into Eq. (10) with re-arrangement gives:

262    $$J_{w(x)} = \frac{\emptyset_{(mix)} \, b}{W} \left(\Delta P_{b(0)} - b \, x \, F_{b(0)} - b \, x \, \Delta P_{b(x)} \left(\emptyset_{(mix)} \right)^{0.5} + b \, x \, \Delta P_{b(0)} \left(\emptyset_{(mix)} \right)^{0.5} \right) \qquad (23)$$

263   Also, another equation for solvent flux can be derived by taking the derivative of Eq. (11)

264   with respect to the x-axis as follows:

265    $$\frac{dJ_{w(x)}}{dx} = \frac{\emptyset_{(mix)} \, b}{W} \left(\frac{d\Delta P_{b(x)}}{dx} \right) \qquad (24)$$

266   Substituting Eq. (12) into Eq. (24) gives:

267    $$\frac{dJ_{w(x)}}{dx} = \frac{\emptyset_{(mix)} \, b}{W} \left(-b \, F_{b(x)} \right) \qquad (25)$$

268   Then, the variation of solvent flux in the x-axis can be calculated by the following equation:

269    $$J_{w(x)} = J_{w(0)} - \left(\frac{\emptyset_{(mix)}}{W} \, b^2 \, x \, F_{b(0)} \right) + \left(\frac{\emptyset_{(mix)}^2 \, b^3}{W} \, \Delta P_{b(0)} \left(\frac{x^2}{2} \right) \right) - \left(\frac{\emptyset_{(mix)}^2 \, b^4}{W} \, F_{b(0)} \left(\frac{x^3}{6} \right) \right) -$$

270    $$\left(\frac{\emptyset_{(mix)}^{2.5} \, b^4}{W} \, \Delta P_{b(x)} \left(\frac{x^3}{6} \right) \right) + \left(\frac{\emptyset_{(mix)}^{2.5} \, b^4}{W} \, \Delta P_{b(0)} \left(\frac{x^3}{6} \right) \right) \qquad (26)$$

271   Where, $J_{w(0)}$ (m/s) is the water flux at the inlet edge of the membrane.

272   Here, it is assumed that the osmotic pressure is caused by the impact of all the species found

273   in sugar (Assumption 5) in contrary to the statement of Álvarez et al. (2001) who neglects

274   both fructose and sorbitol. Therefore, the solvent flux at x = 0 is calculated using Eq. (27)

275   regarding the osmotic pressure, which is caused by sugar compounds (sucrose, glucose, malic

276   acid, fructose and sorbitol).

277    $$J_{w(0)} = A_w \left(\Delta P_{b(0)} - \left(\pi_{su(0)} + \pi_{g(0)} + \pi_{m(0)} + \pi_{f(0)} + \pi_{so(0)} \right) \right) \qquad (27)$$

278 Where, $\pi_{su(0)}, \pi_{g(0)}, \pi_{m(0)}, \pi_{f(0)}$ and $\pi_{so(0)}$ are the osmotic pressure (atm) of sucrose,

279 glucose, malic acid, fructose and sorbitol respectively. The estimation of the osmotic pressure

280 caused by sucrose, glucose and malic acid at any point along the x-axis is carried out using

281 the empirical equation derived by Nabetani et al. (1992b) as can be seen in Eq. (28).

282 $$\pi_{su(x)} + \pi_{g(x)} + \pi_{m(x)} = -\frac{R\,T_b}{V_w}\,ln\left\{\frac{\left[\frac{(1000-C_{w(su)(x)}-C_{w(g)(x)})}{M_{ww}}\right]-\left[\frac{(4\,C_{w(su)(x)})}{M_{su}}\right]-\left[\frac{(2\,C_{w(g)(x)})}{M_g}\right]}{\left[\frac{(1000-C_{w(su)(x)}-C_{w(g)(x)})}{M_{ww}}\right]-\left[\frac{(4\,C_{w(su)(x)})}{M_{su}}\right]-\left[\frac{(2\,C_{w(g)(x)})}{M_g}\right]}\right\}+$$

283 $$\frac{R\,T_b\,C_{w(m)(x)}}{M_m} \qquad (28)$$

284 While, the contribution of fructose and sorbitol to osmotic pressure is calculated by Eqs. (29)

285 and (30).

286 $$\pi_{f(x)} = \frac{R\,T_b\,C_{w(f)(x)}}{M_f} \qquad (29)$$

287 $$\pi_{so(x)} = \frac{R\,T_b\,C_{w(so)(x)}}{M_{so}} \qquad (30)$$

288 Note, all the concentrations expressed in Eqs. (28), (29) and (30) are referred to the

289 concentration of the species at the wall membrane and expressed in (kg/m³).

290 The concentration of the sugar and aroma compounds at the wall membrane was estimated

291 based on Assumption 4, which in turn is based on the validity of the film model theory where

292 the solvent flux is linked to concentration polarization and mass transfer coefficient, k by the

293 following equation:

294 $$\frac{(C_{w(x)}-C_{p(av)})}{(C_{b(x)}-C_{p(av)})} = exp\left(\frac{J_{w(x)}}{k_{(x)}}\right) \qquad (31)$$

295 $C_{b(x)}$, $k_{(x)}$ (kmol/m³, m/s) are the concentration in the feed channel of any species and the

296 mass transfer coefficient respectively.

297 The feed velocity along the x-axis $U_{b(x)}$ (m/s) is calculated by:

298 $$U_{b(x)} = \frac{F_{b(x)}}{W\,t_f} \qquad (32)$$

299 The feed pressure equation can be derived from integration of Eq. (12).

300 $$P_{b(x)} = P_{b(0)} - \left[b\,F_{b(0)}\,x\right] + \left[\emptyset_{(mix)}\,b^2\left(\frac{x^2}{2}\right)\Delta P_{b(0)}\right] - \left[\emptyset_{(mix)}\,b^3\,F_{b(0)}\left(\frac{x^3}{6}\right)\right] -$$

301 $$\left[\emptyset_{(mix)}^{1.5}\,b^3\,\Delta P_{b(x)}\left(\frac{x^3}{6}\right)\right] + \left[\emptyset_{(mix)}^{1.5}\,b^3\,\Delta P_{b(0)}\left(\frac{x^3}{6}\right)\right] \qquad (33)$$

302 The sugar or aroma compounds concentration at the feed channel and at any point along the

303 x-axis is calculated using Eq. (34) as proposed by Lee et al. (2010).

304 $$\frac{d\frac{(C_{b(x)}\,F_{b(x)})}{t_f\,W}}{dx} = -\frac{J_{w(x)}\,C_{p(av)}}{t_f} + \frac{J_{w(x)}\,C_{b(x)}}{t_f} + \frac{d}{dx}\left(D_{(x)}\frac{dC_{b(x)}}{dx}\right) \qquad (34)$$

Then, substituting Eq. (31) and Eq. (8) into Eq. (7) with re-arrangement gives a correlation to calculate the concentration of any sugar or aroma compound at the permeate side. This equation will be used twice at x=0 and x=L as can be shown in Eqs. (35) and (36), and the average solute permeate concentration $C_{p(av)}$ (kmol/m³) is calculated using Eq. (37) as follows:

$$C_{p(0)} = \frac{B_s\, C_{b(0)}\; e^{\frac{J_{w(0)}}{k_{(0)}}}}{J_{w(0)} + B_s\; e^{\frac{J_{w(0)}}{k_{(0)}}}} \tag{35}$$

$$C_{p(L)} = \frac{B_s\, C_{b(L)}\; e^{\frac{J_{w(L)}}{k_{(L)}}}}{J_{w(L)} + B_s\; e^{\frac{J_{w(L)}}{k_{(L)}}}} \tag{36}$$

$$C_{p(av)} = \frac{C_{p(0)} + C_{p(L)}}{2} \tag{37}$$

The volumetric permeated flow rate along the x-axis in the permeate channel can be calculated using Eq. (38):

$$F_{p(x)} = W \int_{x=0}^{x=L} J_{w(x)}\, dx \tag{38}$$

Also, the model facilitates the evaluation of the performance of the unit by calculating the rejection of organic compounds as can be seen in the counter of Eq. (39).

$$Rej = \frac{C_{b(L)} - C_{p(av)}}{C_{b(L)}}\, x100 \tag{39}$$

The recovery of the module calculated using Eq. (40) is the fraction of the feed that is recovered as permeate at the permeate channel. Note that, for a laboratory scale apparatus, the permeate flow rate is small in comparison to feed flow rate.

$$Rec_{(Total)} = \frac{F_{p(Total)}}{F_{b(0)}}\, x100 \tag{40}$$

3.3 The Physical Properties Equations

The mass transfer coefficient is a function of pressure, concentration, flow rate and temperature, which means that k will vary with the membrane length. Schock and Miquel's (1987) correlation is used to estimate the mass transfer coefficient along the x-axis for any species of sugar or aroma compounds as can be depicted in Eq. (41).

$$k_{(x)} = 0.065 \left(\frac{D_{(x)}}{d_h}\right) Re_{b(x)}^{0.875}\; Sc_{(x)}^{0.25} \tag{41}$$

$D_{(x)}$, $Re_{b(x)}$, $Sc_{(x)}$ (m²/s, dimensionless) are the diffusion coefficient of any sugar or aroma compound, the Reynolds number and the Schmidt number of any sugar or aroma compound at any point along the x-axis respectively. The terms can be calculated as follows:

333 $$Re_{b(x)} = \frac{\rho_{b(x)} \, d_h \, U_{b(x)}}{\mu_{b(x)}} \qquad (42)$$

334 $$Sc_{(x)} = \frac{\mu_{b(x)}}{\rho_{b(x)} \, D_{(x)}} \qquad (43)$$

335 Where, $\rho_{b(x)}, \mu_{b(x)}$ and d_h (kg/m³, kg/m s, m) are the apple juice density, viscosity and the

336 hydraulic diameter respectively.

337 The apple juice viscosity can be calculated as a function of concentration in °Brix and

338 temperature using Eq. (44) (Constenla et al., 1989).

339 $$\frac{\mu_{b(x)}}{\mu_w} = exp\left(\frac{A \ °Brix_{(x)}}{100 - B \ °Brix_{(x)}}\right) \qquad (44)$$

340 μ_w and $°Brix_{(x)}$ are the viscosity of water (8.94E-4 kg/m s) and the concentration of apple

341 juice in °Brix. A and B are parameters related to the temperature and can be estimated using

342 Eqs. (45) and (46).

343 $$A = -0.25801 + \frac{817.11}{T_b} \qquad (45)$$

344 $$B = 1.8909 - 3.0212 \, x10^{-3} \, T_b \qquad (46)$$

345 T_b is the absolute temperature.

346 Eq. (47) can be used to calculate the variation of apple juice concentration in °Brix along the

347 length of membrane regarding the concentration of the mixture in kg/m³.

348 $$°Brix_{(x)} = 0.099198 \left(\sum_{i=1}^{n} C_{(x,n)}\right) \qquad (47)$$

349 where, n = Total number of sugar and aroma compounds

350 Where, $C_{(x)}$ (kg/m³) is the concentration of sugar and aroma compounds at any point along

351 the x-axis and calculated using Eq. (48).

352 $$C_{(x,i)} = C_{b(x,i)} \, M_{wt \, (i)} \qquad (48)$$

353 where, i represents the particular species of any sugar or aroma compounds

354 $M_{wt \, (i)}$ (kg/kmol) is the molecular weight of any species under consideration.

355 The apple juice density is calculated using Eq. (49) as a function of concentration in °Brix

356 and temperature (Constenla et al., 1989).

357 $$\rho_{b(x)} = 0.8272 + 0.34708 \exp\left(0.01 \, °Brix_{(x)}\right) - 5.479 \, x10^{-4} \, T_b \qquad (49)$$

358 Then, the diffusion coefficient for any sugar species $D_{SU(x)}$ (m²/s) and aroma compounds

359 $D_{AR(x)}$ (m²/s) along the x-axis can be calculated using the empirical equation proposed by

360 Gladdon and Dole (1953) as can be seen in Eqs. (50) and (51) respectively.

361 $$D_{SU(x)} = D_s \left(\frac{\mu_w}{\mu_{b(x)}}\right)^{0.45} \qquad (50)$$

362 $$D_{AR(x)} = D_a \left(\frac{\mu_w}{\mu_{b(x)}} \right)^{0.45}$$ (51)

363 D_s, D_a (m²/s) are referred to the diffusion coefficient of any species of sugar and aroma

364 compounds respectively in a very dilute solution. These coefficients have been calculated

365 using the proposed correlation of Wilke and Chang (1955).

366 $$D_a = \left(\frac{7.4 \, x10^{-8} \, (2.6 \, M_w)^{0.5} \, (T_b+273.15)}{(1000 \, \mu_{b(x)}) \, (1000 \, V_{bp,A})^{0.6}} \right) x10^{-4}$$ (52)

367 The above equation is correlated to be compatible with the units used. M_w and $V_{bp,A}$

368 (kg/kmol, m³/kmol) are the molecular weight of water and the molar volume of the solute at

369 its normal boiling point. $V_{bp,A}$ values for all sugar and aroma compounds are shown in Table

370 1.

371 Finally, the model presented in this section is built within gPROMS (general Process

372 Modelling System) Model builder, which provides a modelling platform for steady state and

373 dynamic simulation, optimisation, experiment design and parameter estimation of any

374 process.

375

376 **4. Determination of Friction and Transport Parameters**

377 **4.1 Determination of Friction Parameter**

378 Unknown friction parameter of the membrane elements and the operating conditions should

379 be determined before solving the model equations. In the simulation study, experimental data

380 will be used to predict the best values of unknown feed channel friction parameter. These are

381 then used with the known parameters to assess the behaviour of the unit with the variance of

382 operating variables.

383 In this work, the friction parameter has been estimated using an optimization methodology of

384 the gEST parameter estimation tool developed in gPROMS (Process System Enterprise Ltd.,

385 2001). This method has been used on the experimental data of Álvarez et al. (2002) in order

386 to optimize the value of friction parameter. The starting point was based on an initial guess,

387 which was subsequently used to solve the model equations. The preferred value of the

388 friction parameter is reached by continuously varying the predicted value until close fit with

389 experimental data is reached. The registered value of friction parameters for the membrane

390 type MSCB 2521 R99 of effective area 1.03 m² is 90 (atm s/m⁴).

391

392

393

4.2 Determination of Solute Transport Parameters

The solute flux of sugar and aroma compounds through the membrane is given by the product of solute transport parameter and the solute concentration difference at the two channels of the unit as expressed in Eq. (7). So, for calculation purposes, a separate value of the solute transport parameter is required for each species for multiple solutes feed.

4.2.1 Solute Parameters of Aroma Compounds

The solute parameters of aroma compounds B_s (m²/s) for the reverse osmosis module consisting of a spiral-wound aromatic polyamide membrane type (MSCB 2521 R99) were calculated using the equation of Álvarez et al. (2001).

$$B_{s\,i} = B_{s\,i,Ref.}\,exp^{0.098(T_b - T_{Ref.})} \tag{53}$$

i represents the particular species under consideration. $B_{s\,i}$, $B_{s\,i,Ref.}$ and $T_{Ref.}$ are the solute parameter of any aroma compounds at operating temperature (T_b) and the reference temperature of 25 °C ($T_{Ref.}$). Eq. (53) was obtained for a temperature range of 15 °C to 30 °C. The estimated values of solute parameter for each aroma compounds at 25 °C are shown in Table 1.

4.2.2 Solute Parameters of Sugar Compounds

The solute transport parameters B_s (m²/s) of sugar compounds were calculated using the correlation of Matsuura et al. (1976), which assumed the concept of free energy parameter $(-\Delta\Delta G/RT)$ governing non-ionized polar organic solutes in aqueous solution reverse osmosis separation. Eq. (54) shows the general form of this correlation.

$$\ln B_{s\,i} = \ln C_{NaCl}^* + \left(-\frac{\Delta\Delta G}{RT}\right)_i + \delta^* Es^* \tag{54}$$

i represents the particular species under consideration. $\ln C_{NaCl}^*$ is a constant depending on the chemical nature of the membrane and the effective pore size where NaCl as the reference solute. While, the steric Taft number $(\delta^* Es^*)$ is characteristic of each solute in the bulk solution and represents the properties of the solute on the membrane-solution interface and relates to the membrane type.

For the aromatic polyamide membrane type, Matsuura et al. (1976) have found the quantity $\ln C_{NaCl}^*$ using the experimental solute transport parameter data $B_{s\,NaCl}$ for a completely ionized inorganic solute taken NaCl as a reference, and the known values of $(-\Delta\Delta G/RT)$ for both Na^+ and Cl^- ions as can be shown in Eq. (55).

426     $\ln B_{s\,NaCl} = \ln C^*_{NaCl} + \left[\left(-\frac{\Delta\Delta G}{RT}\right)_{cation} + \left(-\frac{\Delta\Delta G}{RT}\right)_{anion}\right]$ (55)

427   Then, the numerical value of (-ΔΔG/RT) for several monovalent inorganic cations and anions

428   in aqueous solutions used in conjunction with aromatic polyamide membrane in reverse

429   osmosis has been obtained using Eq. (56) (Matsuura et al., 1975; Dickson et al., 1975).

430     $\ln B_{s\,NaCl} = \ln C^*_{NaCl} + \left[\left(-\frac{\Delta\Delta G}{RT}\right)_{i}\right]$ (56)

431   While, the free energy parameter of each sugar species (-ΔΔG/RT) and the steric Taft number

432   ($\delta^* Es^*$) of each species of sugar has been calculated by Matsuura et al. (1976) and shown in

433   Table 1.

434   Finally, the transport parameter for each species of sugar for the aromatic polyamide

435   membrane type (MSCB 2521 R99) at 25 °C can be calculated using Eq. (54) as reported in

436   Table 1. However, the transport parameter of malic acid was taken from Malalyandi et al.

437   (1982).

438

439   **5. Model Validation, Results and Discussion**

440   The model described in Section 3 has been validated by comparing the model predictions

441   results with those obtained from actual experimentation for a MSCB 2521 R99 spiral-wound

442   RO aromatic polyamide membrane module carried out by Álvarez et al. (2002). The

443   comparison between the model predictions and experiments is shown in the following

444   section.

445   Figure 1 shows the model rejections of two selected aroma compounds, Isopentyl acetate and

446   *trans*-2-hexanal at two different inlet feed flow rates versus the operating temperature and

447   against experimental results. While, Figures 2 and 3 show the experimental and theoretical

448   results of outlet water flux and feed flow rate versus the operating trans-membrane pressure

449   for different inlet feed flow rates at operating temperature 20 °C.

450   The expectation that increasing inlet feed temperature would increase the solute rejection is

451   validated here as it decreases the viscosity of apple juice as expressed in Eq. (44). This

452   accelerates the flux of water through the membrane and reduces the concentration

453   polarization impact. Interestingly, Figure 1 also shows a slight reduction of Isopentyl acetate

454   and *trans*-2-hexanal rejections with operating temperature for different inlet feed flow rates.

455   The probable explanation for this can be that by increasing the feed temperature, the solute

456   concentration over the membrane wall will increase and causes an increase in solute flux

457   accompanied by the penetrated water that causes an increase in the permeate solute

458   concentration at the permeate channel. As a result, the solute rejection will decrease as

459   expressed in Eq. (39).

460   Furthermore, Figure 1 shows that the model tends to only underestimate the rejection of

461   *trans*-2-hexanal at lower operating temperatures and inlet feed flow rate. This might be

462   attributed to the inaccurate estimation of the transport membrane parameter of *trans*-2-

463   hexanal at such conditions.

464   To illustrate the impact of operating trans-membrane pressure and inlet feed flow rate on

465   solute rejection, Figure 2 shows the variation of Isopentyl acetate rejection versus the

466   operating trans-membrane pressure at three different inlet feed flow rates with comparative

467   data between the model and experiments results. It is expected that the retention of any

468   species will increase due to the increase in operating pressure in turn due to an increase in the

469   water flux passing the membrane. Moreover, the increase of the inlet feed flow rate causes an

470   increase in the Isopentyl acetate rejection due to a reduction in solute flux through the

471   membrane. The increased feed flow rate reduces the wall membrane concentration and causes

472   a decrease of osmotic pressure along the membrane length. Also, an increase in the feed flow

473   rate causes a specific impact on the solute retention by decreasing the amount of accumulated

474   salt on the membrane wall. Consequently, the increasing applied pressure for the same inlet

475   feed flow rate will increase the accumulated salt on the membrane by increasing the water

476   flux.

477   Figure 3 illustrates the effect of operating pressure and inlet feed flow rate in the outlet water

478   flux. The water flux increases due to increase in the operating pressure in line with Eq. (1),

479   which shows that the feed pressure has a substantial impact by bringing up the diffusion rate

480   of water passing through the membrane. Also, it can be noticed that the impact of the inlet

481   feed flow rate is significantly greater at higher operating pressures due to a higher reduction

482   in concentration polarization caused by combining the concurrent impacts of the two feed

483   flow rate and pressure parameters.

484   Similarly, Figure 3 shows that the model predicts the water flux within an accepted error,

485   except at high inlet feed flow rate and operating pressure. This is due to the use of a constant

486   value of water permeability coefficient in all the calculations. It can be argued that this

487   coefficient decreases exponentially with the operating trans-membrane pressure as a result to

488   membrane compaction. At the same time, the water permeability coefficient increases due to

489   an increase in the operating temperature, that causes a reduction in water viscosity. It is

490   expected that these reasons contribute to the slight discrepancy between the outputs of the

491   model and experiments at these conditions.

The clear corroboration with experimental data readily shows the suitability of the model to measure the observed retention and water flux parameters with an accepted error over the operating ranges of trans-membrane pressures and temperatures.

Figure 4 shows the consistence between the model prediction and experiments results for the outlet feed flow rate versus the operating trans-membrane pressure using three different inlet feed flow rates.

Figure 5 shows the effect of operating trans-membrane pressure in the outlet °Brix for different inlet feed flow rates. It is expected that the concentration in °Brix will increase due to an increase in the operating pressure. This is due to the increase in water flux by increasing the operating pressure. The concentration in °Brix that can be obtained is limited to the range 10.55 – 11.32 of used pressure and this might be attributed to the use of small specific area of membrane module.

It is also interesting to notice that the outlet concentration in °Brix is almost the same for all three inlet feed flow rates at lower inlet operating pressure. However, there is a noted discrepancy at higher operating pressures. Overall, the concentration in °Brix decreases due to an increase in the operating feed flow rate, especially when using higher operating pressures in spite of increasing water flux with increasing inlet feed flow rate, as more specifically illustrated in Figure 3. The reason for this phenomenon is that increasing inlet feed flow rate results in increasing the mass transfer coefficient and decreasing the concentration polarization. Also, the increased feed flow rate reduces the wall membrane concentration and causes a decrease of osmotic pressure, which is followed by decreasing sugar and aroma compounds concentration along the membrane due to a better mixing in the feed channel.

Figure 6 displays the variation of operating temperature within the permissible limits of the manufacturer's specifications of the module as a function of apple juice concentration measured in °Brix. It can be observed that the concentration increases as a result to increase in the operating temperature. In line with Eq. (2), the water permeability coefficient increases with increasing the operating temperature, which causes an increase in water flux that raises the apple juice concentration in the feed side.

Finally, a 10% maximum error agreement is obtained in a comparison between experimental and calculated rejection for all aroma compounds as presented in Figure 7. The relatively small discrepancy can be attributed to two reasons. Firstly, the actual experiments of Álvarez et al. (2002) is carried out using apple juice concentration of 11 °Brix not 10.5 °Brix.

525 Secondly, constant solute transport parameters of aroma compounds are used in the
526 calculation of solute flux through the membrane as can be seen in Eq. (7).

527

528 **Conclusions**

529 A mathematical one dimensional steady model applicable for apple juice concentration
530 process using a spiral-wound reverse osmosis process has been developed with a simulation
531 study of permeate flux and aroma compounds rejection. The model can predict the variation
532 of the feed flow rate, sugar and aroma compounds concentration in both the feed and
533 permeate channels, membrane wall concentration, feed pressure and water and solute fluxes
534 in each point along the membrane length. A number of differential equations have been
535 developed based on the solution-diffusion model, which takes into account the impact of all
536 sugar species in the calculation of osmotic pressure. Besides, the model estimates the
537 physical properties of apple juice using the empirical equations that shows the impact of
538 concentration and temperature derived from the literature. Also, the solute transport
539 parameters of sugar species were determined based on the concept of free energy parameter.
540 The model has been validated against an experimental data set derived from an apple juice
541 concentration process and shows accepted relative errors between theoretical and
542 experimental results for most operating parameters. The model has been used for further
543 simulation to study the influence of various operating conditions on permeate flux and aroma
544 compounds rejection. Further work is planned to optimize the apple juice concentration and
545 aroma compound retention by assessing the impact of module area and operating variables.

546 **References**

547 Álvarez V., Álvarez S., Riera F., and Álvarez R., 1997. Permeate flux prediction in apple
548   juice concentration by reverse osmosis. Journal of Membrane Science, 127, 25-34.

549 Álvarez S., Riera F., Álvarez R. and Coca J., 1998. Permeation of apple juice compounds in
550   reverse osmosis. Separation Purification Technology, 14, 209-220.

551 Álvarez S., Riera F., Álvarez R. and Coca J., 2001. Prediction of flux and aroma compounds
552   rejection in a reverse osmosis concentration of apple juice model solutions. Ind. Eng.
553   Chem. Res., 40, 4925-4934.

554 Álvarez S., Riera F., Álvarez R. and Coca J., 2002. Concentration of apple juice by reverse
555   osmosis at laboratory and pilot-plant scales. Ind. Eng. Chem. Res., 41, 6156-6164.

556   Cheong K. W.,Tan C. P., Mirhosseini H., Abdul Hamid N. S., Osman A. and Basri M., 2010.
557   Equilibrium headspace analysis of volatile flavor compounds extracted from soursop
558   (Annona muricata) using solid-phase microextraction. Food Research International,
559   43(5), 1267-1276.

560   Dickson J. M., Matsuura T., Blais P. and Sourirajan S., 1975. Reverse osmosis separation in
561   some organic and inorganic solutes in aqueous solutions using aromatic polyamide
562   membranes. Journal of Applied Polymer Science, 19, 801-819.

563   Gladdon J. K. and Dole M., 1953. Diffusivity determination of sucrose and glucose solutions.
564   J. Am. Chem. Soc., 75, 3900-3904.

565   Constenla D. T., Lozano J. E. and Crapiste G. H., 1989. Thermo-physical properties of
566   clarified apple juice as a function of concentration and temperature. J. Food Sci., 54(3),
567   663-668.

568   Girard B. and Fukumoto L. R., 2000. Membrane processing of fruit juices and beverages: A
569   review. Critical Reviews in Food Science and Nutrition, 40(2), 91-157.

570   Jain S. and Gupta S. K., 2004. Analysis of modified surface force pore flow model with
571   concentration polarization and comparison with Spiegler–Kedem model in reverse
572   osmosis systems. Journal of Membrane Science, 232(1-2), 45-62.

573   Jiao B., Cassano A. and Drioli E., 2004. Recent advance on membrane processes for the
574   concentration of fruit juices: A review. Journal of Food Engineering, 63, 303-324.

575   Lee C., Chen Y. and Wang G., 2010. A dynamic simulation model of reverse osmosis
576   desalination systems. The 5th International Symposium on Design, Operation and
577   Control of Chemical Processes, PSE Asia, Singapore.

578   Lonsdale H. K., Merten U. and Riley R. L., 1965. Transport properties of cellulose acetate
579   osmotic membranes. Journal of Applied Polymer Science, 9, 1341-1362.

580   Malalyandi P., Matsuura T. and Sourirajan S., 1982. Predictability of membrane performance
581   for mixed solute reverse osmosis systems. System cellulose acetate membrane-D-
582   Glucose-D,L-Malic acid-water. Ind. Eng. Chem. Process. Dev., 21, 277-282.

583   Matsuura T., Bednas M. E., Dickson J. M. and Sourirajan S., 1974. Polar and steric effects in
584   reverse osmosis. Journal of Applied Polymer Science, 18, 2829-2846.

585   Matsuura T., Bednas M. E., Dickson J. M. and Sourirajan S., 1975. Reverse osmosis
586   separations of aldehydes, ketones, and ethers in aqueous solutions using porous
587   cellulose acetate membranes. J. Appl. Polym. Sci., 19(9), 2473-2484.

588   Matsuura T., Dickson J. M. and Sourirajan S., 1976. Free energy parameters for reverse
589   osmosis separations of undissociated polar organic solutes in dilute aqueous solutions.
590   Ind. Eng. Chem. Process Des. Dev., 15(1), 149-161.

591   Nabetani H., Nakajima M., Watanabe A., Ikeda S., Nakao S. and Kimura S., 1992a.
592   Development of a new type of membrane osmometer. Journal of Chemical Engineering
593   of Japan, 25, 269-274.

594   Nabetani H., Nakajima M., Watanabe A., Nakao S. and Kimura S., 1992b. Prediction of the
595   flux for the reverse osmosis of a solution containing sucrose and glucose. Journal of
596   Chemical Engineering of Japan, 25(5), 575-580.

597   Pereira E. N., Matsuura T. and Sourirajan S., 1976. Reverse osmosis separations and
598   concentrations of food sugars. J. Food Sci., 41, 672.

599   Pepper D., 1990. RO for improved products in the food and chemical industries and water
600   treatment. Desalination, 77, 55-71.

601   Pozderovic´ A., Moslavac T. and Pichler A., 2006. Concentration of aqueous solutions of
602   organic components by reverse osmosis II. Influence of transmembrane pressure and
603   membrane type on concentration of different alcohol solutions by reverse osmosis.
604   Journal of Food Engineering, 77, 810-817.

605   Process System Enterprise Ltd, 2001. gPROMS Introductory User Guide. Process System
606   Enterprise Ltd., London.

607   Sheu M. and Wiley R., 1983. Preconcentration of apple juice by reverse osmosis. Journal of
608   Food Science, 48(2), 422-429.

609   Schock G. and Miquel A., 1987. Mass transfer and pressure loss in spiral wound modules.
610   Desalination, 64, 339-352.

611   Wilke C. R. and Chang P., 1955. Correlation of diffusion coefficients in dilute solutions.
612   A.I.Ch.E. Journal, 1(2), 264-270.

613

614

615

616 Table 1: Characteristics of the sugar and aroma compounds and their inlet concentration in the model solution of

617 10.5 °Brix (Matsuura et al., 1976; Álvarez et al., 1998; Malalyandi et al., 1982; Álvarez et al., 2002)

Compound	Molecular weight M_{wt}, (kg/kmol)	Concentration $C_{b(0)}$, (kmol/m³)	Molar volume, $V_{bp,A}$ (m³/kmol)	Free energy parameter, $(-\frac{\Delta\Delta G}{RT})_{25\,°C}$	Steric Taft number, $(\delta^*Es^*)_{25\,°C}$	Solute transport parameter, $B_{s,25\,°C}$ (m/s)
sucrose	342	0.035555	0.215689	-1.76	-7.42	2.32996E-10
glucose	180	0.138000	0.116987	1.81	-5.42	6.11461E-8
malic acid	134	0.029104	0.083337	---	---	5.40E-8
fructose	180	0.340722	0.106351	1.59	-5.56	4.26602E-8
sorbitol	182	0.018406	0.122343	1.82	-5.57	5.31579E-8
ethyl acetate	88.11	0.000566	0.097683	2.11	-0.07	4.818E-6
ethyl butanoate	116.16	0.000129	0.132150	1.54	-0.43	1.739E-6
ethyl-2-methyl butanoate	130.19	5.37E-05	0.150508	1.47	-1.20	0.223E-6
isopentyl acetate	130.19	0.000130	0.148618	1.47	-0.35	0.387E-6
Hexyl acetate	144.22	6.926E-05	0.166274	1.85	-0.40	1.564E-6
trans-2-hexenal	98.143	0.000712	0.116004	---	---	4.574E-6
hexanal	100.2	0.000149	0.123095	2.19	-0.40	2.084E-6
isobutanol	74.12	0.000269	0.092421	2.42	-0.93	0.302E-6
butanol	74.12	0.000269	0.091506	2.17	-0.39	1.905E-6
isopentanol	88.15	0.000169	0.108771	2.12	-0.35	0.297E-6
hexanol	102.18	0.000293	0.125522	2.81	-0.40	1.556E-6

618

619 Table 2: Specifications of the spiral-wound membrane element (Álvarez et al., 2002)

| *Make*	*Sparem Spa. (Biella, Italy)*
Membrane type and configuration	MSCB 2521 R99, Spiral-wound, Polyamide membrane
Active surface area (m²)	1.03
Feed and permeate spacer thickness (t_f) and (t_p) (m)	0.0007 and 0.00055
Membrane sheet length (L) and width (W) (m)	0.44 and 2.3409
Hydraulic diameter (m)	0.00096
Max. operating pressure (atm)	41.4508
Max. operating temperature (°C)	50

620

621

622
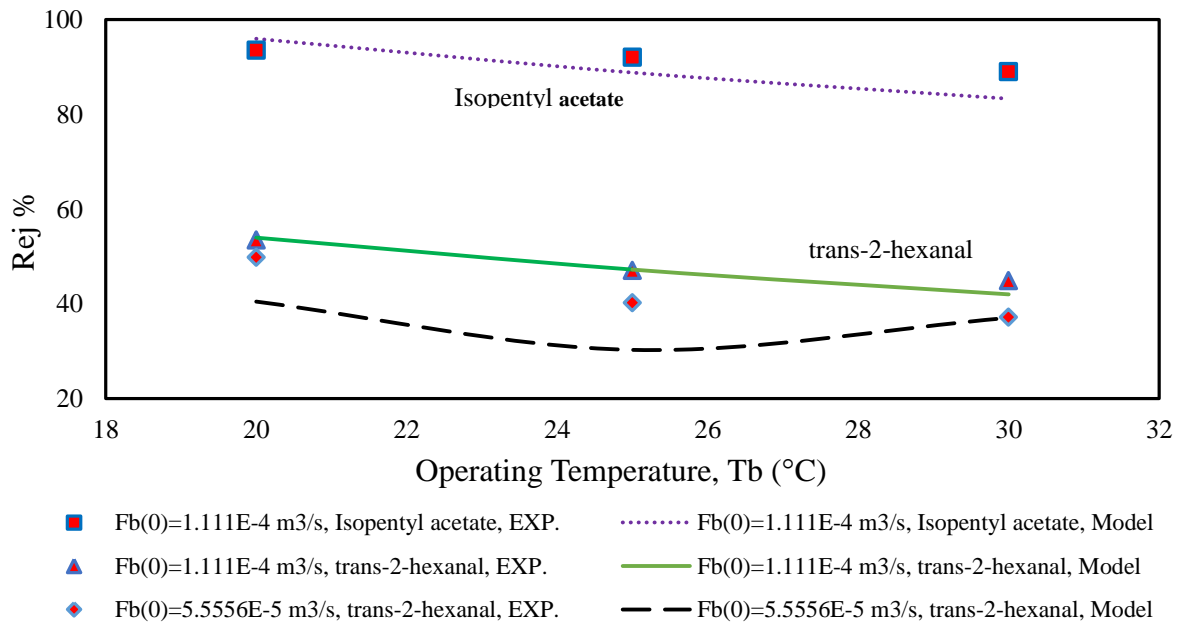
Figure 1: Experimental and model rejections of the two selected aroma compounds versus average operating temperature for two different inlet feed flow rates at inlet conditions (°Brix = 10.5, TMP = 34.542 atm)
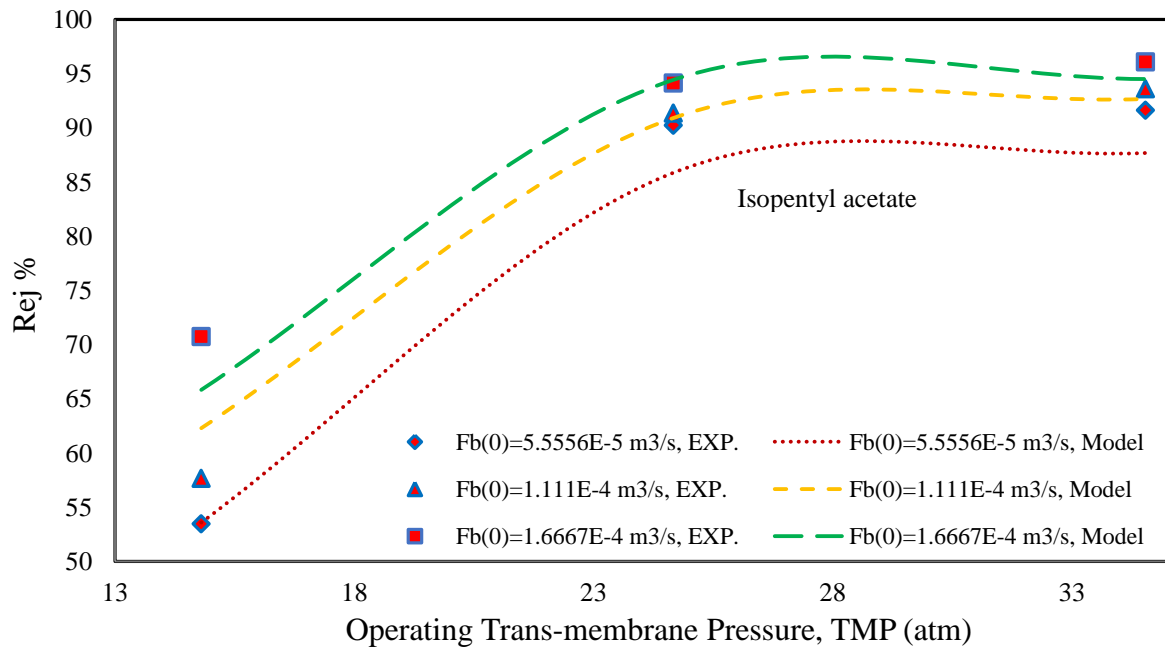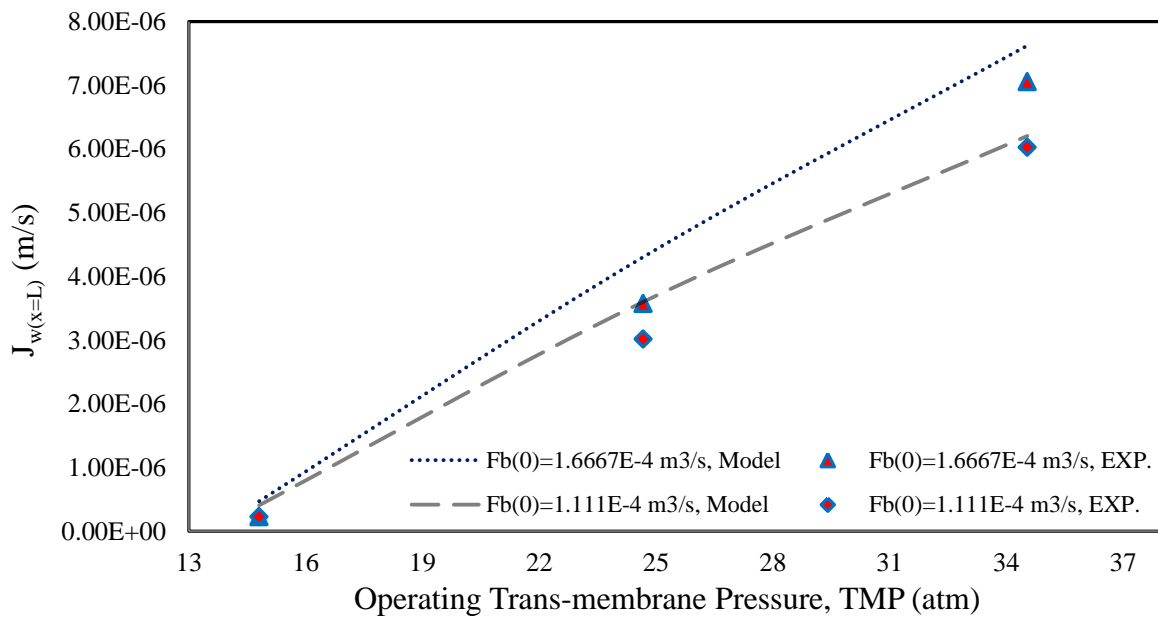

Figure 2: Experimental and model Isopentyl acetate rejection versus operating trans-membrane pressure for three different inlet feed flow rates at inlet conditions (°Brix = 10.5, T_b = 20 °C)
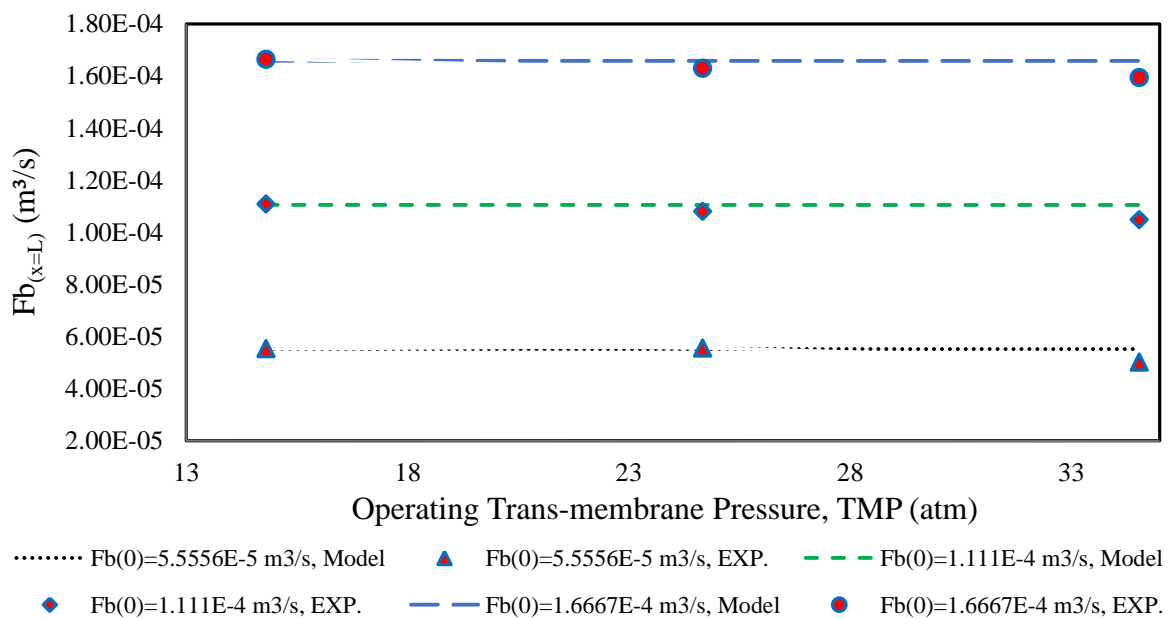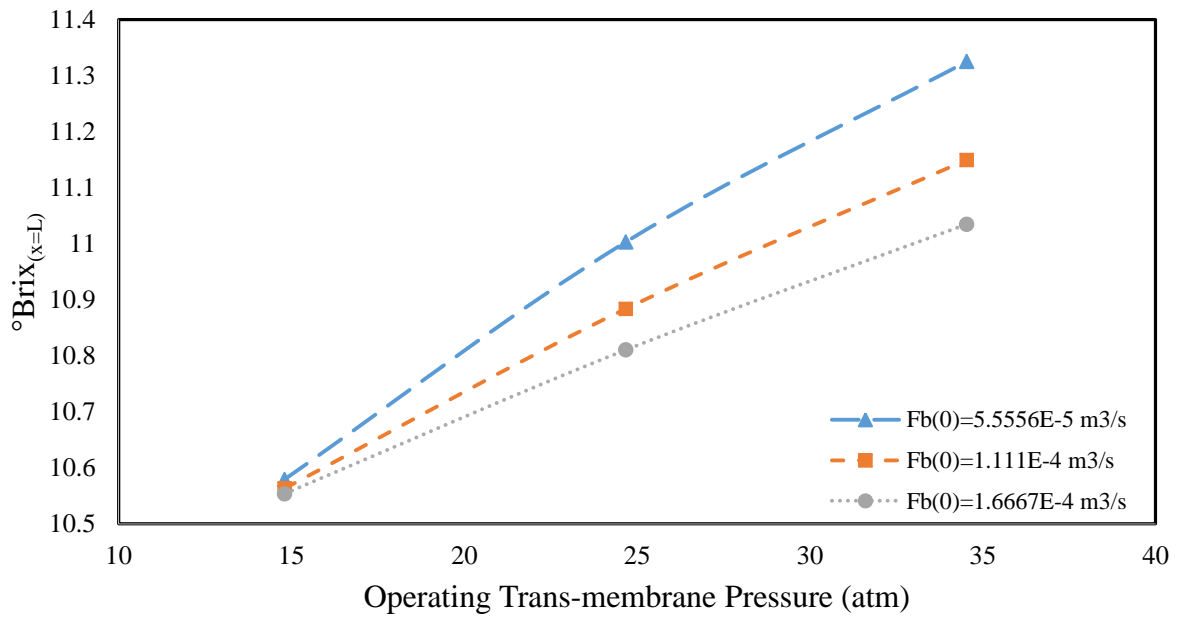
635

636

Figure 3: Experimental and model outlet water flux versus operating trans-membrane pressure for two different inlet feed flow rates at inlet conditions (°Brix = 10.5, $T_b = 20$ °C)

637
638

639

640

641

642 Figure 4: Experimental and model outlet feed flow rate versus operating trans-membrane pressure for three
643 different inlet feed flow rates at inlet conditions (°Brix = 10.5, $T_b = 20$ °C)
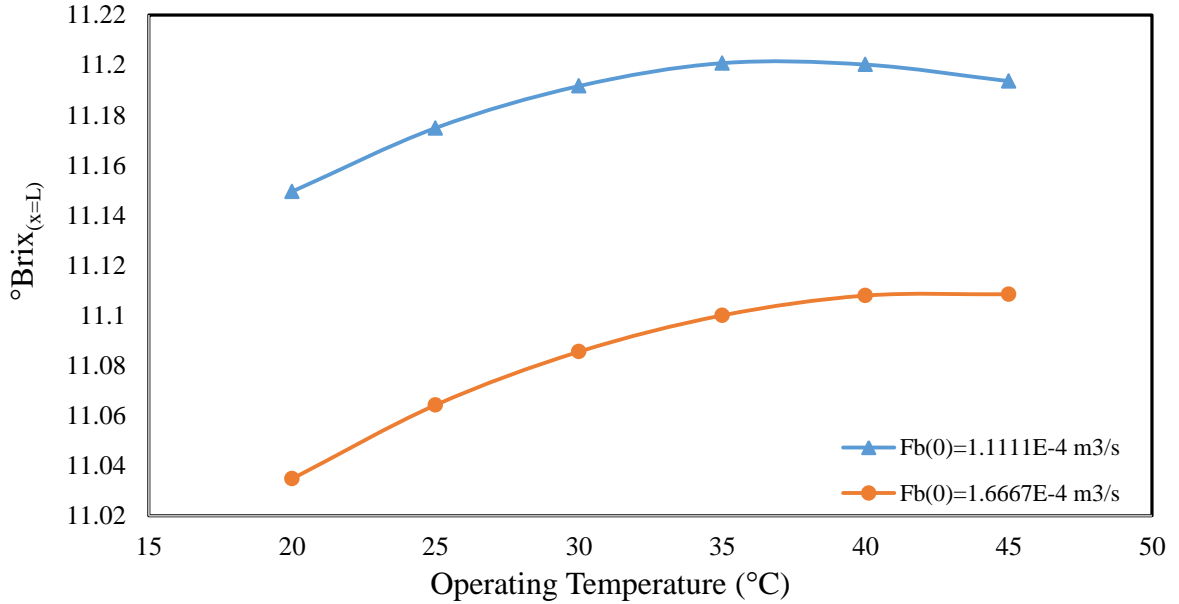
644

645

646

649   Figure 5: Outlet Brix variation as a function of operating trans-membrane pressure at different inlet feed flow
650   rates at inlet conditions (°Brix = 10.5, $T_b = 20$ °C)

651

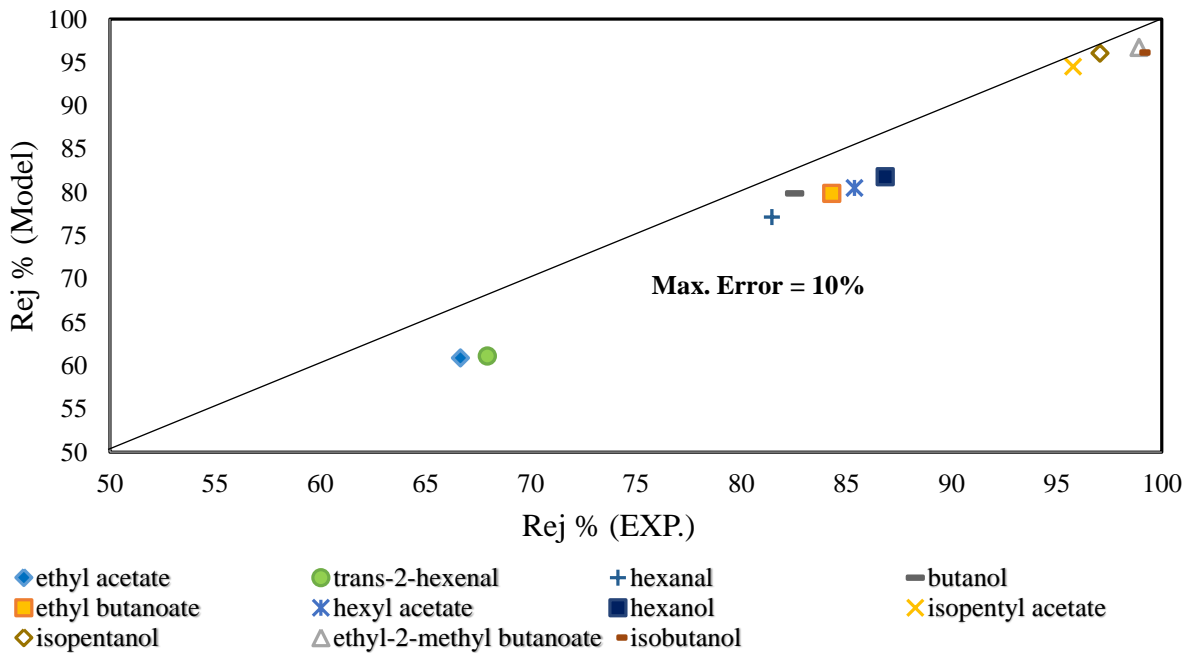652

654   Figure 6: Outlet Brix variation as a function of operating temperature at different inlet feed flow rates at inlet
655   conditions (°Brix = 10.5, $TMP = 34.542$ atm)

656

657

658

659

Figure 7: Experimental and predicted aroma compounds rejection at inlet conditions (°Brix = 10.5, T_b = 20 °C, TMP = 34.542 atm, $F_{b(0)}$ = 1.6667E-4 m³/s)

660

661

662

663

664